Received: 17 June 2022 | Revised: 17 August 2022 | Accepted: 20 September 2022

DOI: 10.1002/hbm.26103

RESEARCH ARTICLE

WILEY

Highly connected and highly variable: A Core brain network during resting state supports Propofol-induced unconsciousness

Siyang Li[1,2] | Yali Chen[3] | Peng Ren[1] | Zhipeng Li[1,2] | Jun Zhang[3,4] | Xia Liang[1,2]

[1]School of Life Science and Technology, Harbin Institute of Technology, Harbin, China

[2]Laboratory for Space Environment and Physical Sciences, Harbin Institute of Technology, Harbin, China

[3]Department of Anesthesiology, Shanghai Cancer Center, Fudan University, Shanghai, China

[4]Department of Oncology, Shanghai Medical College, Fudan University, Shanghai, China

Correspondence
Xia Liang, Laboratory for Space Environment and Physical Sciences, Harbin Institute of Technology, Harbin 150001, China.
Email: xia.liang@hit.edu.cn

Jun Zhang, Department of Anesthesiology, Shanghai Cancer Center, Fudan University, Shanghai 200032, China.
Email: snapzhang@aliyun.com

Funding information
Central University Basic Research Fund of China, Grant/Award Number: HIT. NSRIF. 2020042; National Natural Science Foundation of China, Grant/Award Numbers: 81671769, 82072000, 82171261; Natural Science Foundation of Heilongjiang Province, Grant/Award Number: LH2019H001

Abstract

Despite that leading theories of consciousness make diverging predictions for where and how neural activity gives rise to subjective experience, they all seem to partially agree that the neural correlates of consciousness (NCC) require globally integrated brain activity across a network of functionally specialized modules. However, it is not clear yet whether such functional configurations would be able to identify the NCC. We scanned resting-state fMRI data from 21 subjects during wakefulness, propofol-induced sedation, and anesthesia. Graph-theoretical analyses were conducted on awake fMRI data to search for the NCC candidates as brain regions that exhibit both high rich-clubness and high modular variability, which were found to locate in prefrontal and temporoparietal cortices. Another independent data set of 10 highly-sampled subjects was used to validate the NCC distribution at the individual level. Brain module-based dynamic analysis revealed two discrete reoccurring brain states, one of which was dominated by the NCC candidates (state 1), while the other state was predominately composed of primary sensory/motor regions (state 2). Moreover, state 1 appeared to be temporally more stable than state 2, suggesting that the identified NCC members could sustain conscious content as metastable network representations. Finally, we showed that the identified NCC was modulated in terms of functional connectedness and modular variability in response to the loss of consciousness induced by propofol anesthesia. This work offers a framework to search for neural correlates of consciousness by charting the brain network topology and provides new insights into understanding the roles of different regions in underpinning human consciousness.

KEYWORDS
consciousness, dynamic states, modular variability, neural correlates of consciousness, rich-club

Siyang Li and Yali Chen equally contributed to this work.

1 | INTRODUCTION

Consciousness is what we experience subjectively every day when a salient external stimulus accesses conscious operation, or when our minds spontaneously wander into episodic memory. While mounting evidence suggests the existence of the neural correlates of consciousness (NCC), it is not clear yet where especially they are located in the brain (Hawrylycz et al., 2015). Different theories of consciousness make diverging predictions for where and how neural activity gives rise to subjective experience (Boly et al., 2017; Mashour, 2018; Melloni et al., 2021; Odegaard et al., 2017). For example, the Global Neuronal Workspace Theory (GNWT) states that the prefrontal cortex plays a crucial role in consciousness (Dehaene et al., 2011; Dehaene & Changeux, 2011; Mashour et al., 2020), and the integrated information theory (IIT) postulates that the posterior hot zones of the temporo-parieto-occipital areas are sufficient to mediate consciousness (Tononi et al., 2016), and the Temporo-spatial Theory of Consciousness (TTC) tends to favor a more globally distributed substrate for consciousness (Northoff & Huang, 2017; Northoff & Lamme, 2020; Northoff & Zilio, 2022b).

Despite various distinctions among these influential theories of consciousness, they seem to partially agree on an account that the neural correlates of consciousness require to support globally integrated brain activity across a network of functionally specialized modules (Brown et al., 2019; Dehaene et al., 2011; Dehaene & Changeux, 2011; Oizumi et al., 2014; Tononi, 2004). Indeed, prior studies estimating brain integration based on graph-theoretical tools have confirmed the reduction in brain-wide global synchronization under diverse general anesthetics and in patients with disorders of consciousness (Alkire et al., 2008; Boly et al., 2008; Boveroux et al., 2010; Dehaene et al., 2011; Dehaene & Changeux, 2011; Laureys et al., 2002; Lee et al., 2013; Lee & Mashour, 2018; Mhuircheartaigh et al., 2010; Schrouff et al., 2011). In contrast, activities of functional separated modules, another important aspect involved in the information integration process during the conscious experience, have received little attention in previous studies searching for the neural correlates of consciousness. The brain's modular structure represents groups of densely connected regions with shared functionality (Meunier et al., 2010; Power et al., 2011; Sporns & Betzel, 2016; Yan & He, 2011) and has become the focus of various investigations. By demonstrating remarkable temporal and individual variability in the spatial topography of brain modules (Cavanna et al., 2018; Cui et al., 2020; He et al., 2018; Li et al., 2019; Liao et al., 2017; Shine & Poldrack, 2018), recent studies have suggested that variability in modular topography reflects flexible adaptation to changing environments and underlies individual differences in cognitive and behavioral capacity (Cui et al., 2020; Shine & Poldrack, 2018). However, the relevance of a region's modular variability to its role in consciousness remains an open question. Given the evidence that regions with higher modular variability are more likely to be reassigned depending on the mental context (Cohen & D'Esposito, 2016; Shine & Poldrack, 2018), consciously accessible experiences fluctuating over time or among individuals would require diversified representations supported by diverse module patterns. We, therefore, hypothesize that, apart from the centralized connectivity architecture, neural correlates of consciousness should also be characterized by higher variability of modular affiliations in response to various external stimuli, or to the stream of spontaneous thoughts during wakeful resting state.

To test our hypothesis, we aimed to locate neural correlates of consciousness by analyzing two critical organizational aspects, that is, rich-clubness and modular variability, of spontaneous brain activity from resting-state fMRI data. We searched for NCC candidates by identifying brain regions with both high rich-clubness and high modular variability in a cohort of 21 subjects during awake resting state, and validated at the individual level in another independent data set of 10 highly-sampled subjects. We also explored the dynamics of spontaneous brain networks and hypothesized that the identified NCC candidates should be more involved in a temporally more stable state. To further demonstrate the linkage between NCC candidates and conscious processing, we analyzed fMRI data during propofol administration with varying concentrations and hypothesized that the NCC regions would be more sensitive to general anesthetic-induced loss of consciousness.

2 | MATERIAL AND METHODS

2.1 | Anesthesia dataset

Twenty-one patients (male/female: 9/12; age: 32–64 years) who were selected for elective resection of pituitary microadenoma via a transsphenoidal approach (<10 mm in diameter without sella expansion by radiological and plasma endocrine indicators) attended the experiments. The participants had American Society of Anesthesiologists physical status I-II grade and no history of craniotomy, cerebral neuropathy, vital organ dysfunction, or administration of neuropsychiatric drugs within three months. In addition, these patients had no neuropsychiatric and cognitive abnormality in preoperative evaluation. Moreover, the pituitary microadenomas were diagnosed by their size (<10 mm in diameter without sella expansion) based on radiological examinations and plasma endocrinal indicators. The procedure was approved by the institutional review board of Huashan Hospital, Fudan University (ethics review number: KY2015-273). All participating subjects provided written informed consent before enrollment. For more details, please refer to our previous work (Huang et al., 2018; Huang et al., 2020; Tanabe et al., 2020).

2.2 | Anesthesia protocol

The participants received propofol sedation and deep anesthesia, during which intravenous anesthetic propofol was infused through an intravenous catheter placed into a vein of the right hand or forearm. Propofol was administered using a target-controlled infusion (TCI) pump to obtain constant effect-site concentration, as estimated by the pharmacokinetic model (Marsh et al., 1991). Remifentanil (1.0 μg/kg) and succinylcholine (1.5 mg/kg) were administered to facilitate

endotracheal intubation at deep anesthesia. The TCI propofol was maintained at a stable effect-site concentration of 1.3 μg/ml for sedation, and 4.0 μg/ml for deep anesthesia, which could reliably induce an unconscious state (Xu et al., 2009). A 5-min equilibration period was allowed to insure equilibration of propofol repartition between compartments. The level of consciousness was evaluated clinically by asking the subject to strongly squeeze the hand of the investigator with the Ramsay sedation scale (Ramsay et al., 1974). The corresponding Ramsay scores (median with 1st, 3rd quartile) for 1.3 μg/ml of propofol effect-site concentration was 4.0 (2.0, 5.0), which was considered as moderate sedation state; and for 4.0 μg/ml was 6.0 (6.0, 6.0), considered as anesthesia state (loss of consciousness). In the postoperative follow-up, no subject reported intraoperative awareness during the fMRI scanning and surgical procedure. Detailed anesthesia protocol has been described in our previous work (Huang et al., 2018).

2.3 | Image acquisition

Participants were scanned on a Siemens 3 T scanner (Siemens MAGNETOM, Germany) to acquire high-resolution T1-weighted anatomical images (echo time (TE) = 5 ms, repetition time (TR) = 1000 ms, slice thickness = 1.0. mm, 176 slices, image size = 448 × 512, FOV = 219 × 250 mm^2, flip angle = 90°) and resting-state fMRI images using gradient-echo echo-planar imaging (EPI) sequence (TE = 30 ms, TR = 2000 ms, slice thickness = 5.0 mm, number of slices = 33, repetition = 240, image size = 64 × 64, FOV = 210 × 210 mm^2, flip angle = 90°). Resting-state fMRI images were scanned eyes-closed for 8 min during wakefulness, sedation, and general anesthesia, respectively. Before sedation scanning, the subjects were administered 500 ml intravenous hydroxyethyl starch to prevent hypotension caused by propofol-induced vasodilation.

A secondary, independent data set including fMRI images from ten subjects was downloaded from the Midnight Scan Club website (MSC, https://legacy.openfmri.org/dataset/ds000224/) for validation. Briefly, the participants were scanned on a Siemens 3.0 T Tim Trio (software version syngo MR B17) to acquire high-resolution T1-weighted anatomical images (TE = 3.7 ms, TR = 2400 ms, slice thickness = 0.801 mm, 256 slices, image size = 224 × 256, FOV = 179 × 205 mm^2, flip angle = 8°) and resting-state fMRI images using gradient-echo echo-planar imaging (EPI) sequence (TE = 27 ms, TR = 2200 ms, slice thickness = 4.0 mm, number of slices = 36, repetition = 818, image size = 64 × 64, FOV = 256 × 256 mm^2, flip angle = 90°). Resting-state fMRI images were scanned eyes-open for 30 min per session, totaling 300 min per subject. Details of the MSC data set are published elsewhere (Gordon et al., 2017).

2.4 | fMRI image processing

Resting-state fMRI images from the anesthesia data set were preprocessed using AFNI (Analysis of Functional Neuroimages) (Cox, 1996). After discarding the first five frames, fMRI images were corrected for different slice timing, realigned, coregistered with the high-resolution anatomical images, and spatially normalized to the standard template brain (Talaraich stereotactic space). Head motion and signals from the white matter and cerebrospinal fluid were regressed out to control for physiological and non-neural noise. Band-pass filtering (0.01–0.1 Hz) and spatial smoothing (6 mm FWHM) were then applied. Since the human subjects underwent fMRI scans from wakefulness to anesthesia, the head motions tend to be larger while awake; to mitigate motion-related confounding, subjects with extra head motions under any of three conditions were discarded from further analyses (remaining 17 subjects) (Power et al., 2012; Yan et al., 2013). The exclusion criteria included: (1) averaged head translation/rotation >3 mm/3°; (2) 4-min longer time points with frame-wise displacement (FD) >0.7 mm.

For the MSC validation data set, preprocessed fMRI images were downloaded directly from the MSC website. Note that one subject is reported repeatedly falling asleep and exhibited several non-negligible eye closures, along with increasing head motion (Gordon et al., 2017), thus was excluded, remaining nine subjects for further analyses.

2.5 | Static functional network construction

To construct functional brain networks, we first parcellated the brain according to a predefined brain atlas, which yielded 246 regions of interest (ROI) (Fan et al., 2016). For each subject, we averaged the voxel-wise time course within each region and computed the Pearson correlation to obtain functional connectivity (FC) matrix. A density threshold of S = 15% was applied to remove as many spurious correlations as possible while maintaining fully connected brain networks.

2.6 | Dynamic functional network construction

Dynamic FC was estimated using a sliding window approach. We used a window length of 25 TRs slides in steps of 1 TR individually, resulting in 211 time windows (TWs) at each of the three conscious levels for the propofol anesthesia data set and 8156 TWs for the validation data set. We then calculated the Pearson's correlation coefficients for each pair of regions from the windowed time course segments. The resulting windowed correlation matrices were thresholded using connectivity densities of 15% to generate dynamic functional networks.

2.7 | Rich club analysis

The rich-club organization represents a core set of highly-connected regions that are more densely interconnected in a network. To detect rich-club organization in a weighted network, we first computed the FC strength of each brain region as the average of FC with all the other regions, and calculated the rich-club coefficient as follows (Colizza et al., 2006; Opsahl et al., 2008):

$$\emptyset^{\omega}(s)=\frac{\omega_{>s}}{\sum_{l=1}^{E_{>s}}W_l^{rank}},$$

where $\omega_{>s}$ is the sum of connectivity strength between nodes with nodal strength higher than s, $E_{>s}$ is the number of these connections, and W_l^{rank} is the sum of the top $E_{>s}$ strongest connectivity across the network. By dividing $\emptyset^{\omega}(s)$ by $\emptyset^{\omega}_{rand}(s)$, a normalized $\emptyset^{\omega}_{norm}(s)$ is generated, where $\emptyset^{\omega}_{rand}(s)$ is the averaged rich-club coefficient of 1000 random networks with the same nodal degree and strength distribution. A network appears to have the rich-club organization if $\emptyset^{\omega}_{norm}(s) > 1$ for a continuous range of s. The permutation test was performed to assign a P value at each s by comparing the observed $\emptyset^{\omega}(s)$ with the null distribution of $\emptyset^{\omega}_{rand}(s)$ obtained from random networks. Bonferroni method was used to correct multiple comparisons.

2.8 | Modular structure detection

We assessed the modular structure by applying modularity analysis on static or dynamic brain networks (Blondel et al., 2008; Newman & Girvan, 2004; Sporns & Betzel, 2016). To achieve an optimal module partition, we applied a two-step procedure similar to that described by Rubinov and Sporns (2011). Briefly, the modular partition was first estimated using the Louvain algorithm 100 times, followed by a fine-tuning algorithm that was performed repeatedly until the modularity of the partition no longer increased; a consensus partition was then identified with the highest modularity. To choose an appropriate value for the resolution γ parameter in the modularity analysis, we repeated the above two-step procedure across a range of γ values (1–2 in steps of 0.1); for the modular partition obtained for each γ value, we computed the variation of information (VI) with those identified at the neighboring γ values, and γ parameter with the lowest VI was selected as it provides the most robust estimates of topology across these iterations (He et al., 2018; Sporns & Betzel, 2016).

2.9 | Modular variability

To estimate the variability of spatial affiliations between different modular partitions, for a given brain region *k*, we calculated the modular variability (MV) between modular affiliation *i* and *j* obtained in different subjects or time windows as follows (Liao et al., 2017; Steen et al., 2011):

$$MV_k(i,j)=1-\frac{|M_i\cap M_j|}{|M_i|}\times\frac{|M_i\cap M_j|}{|M_j|},$$

where M_i and M_j denote the module label to which region *k* belongs in modular partitions *i* and *j*, respectively. $M_i\cap M_j$ represents the mutual region set between modules M_i and M_j, and $|M_i\cap M_j|$ denotes the number of regions in the common region set. $|M_i|$ and $|M_j|$ denote the number of regions in modules M_i and M_j, respectively. The average modular variability for node *k* across all *n* modular partitions can then be calculated as:

$$MV_k=\frac{1}{n}\times\sum_{i=1}^{i=n}MV_{k,i},$$

where $MV_{k,i}=\frac{1}{n-1}\times\sum_{j\neq i}MV_k(i,j)$ denotes the modular variability for region *k* between modular partition *i* and all other partitions.

2.10 | Dynamic state detection

Recent evidence suggested that fluctuations of neuronal activity could be characterized by highly structured connectivity patterns that reoccur over time, which have been described as "brain states" (Allen et al., 2014; Cribben et al., 2012; Yang et al., 2014; Yu et al., 2015). Since the present study focused on the spatial variability of modular organization, we developed a new method to detect brain states at individual and group levels based on the temporal variability of modular structure in functional brain networks.

To identify dynamic states in each individual during different levels of responsiveness, we first detected the modular structures of each time-varying brain network using the Louvain modularity algorithm in GRETNA toolbox (Wang et al., 2015). To estimate the similarity of modular structures between different TWs, for each brain region *k*, we generated a similarity matrix, $iMV(w\times w)$, by inversing the across-time $MV_k(i,j)$ values (w: number of time windows). Modularity analysis was then applied to this similarity matrix, $iMV(w\times w)$, to identify modules that might correspond to sets of TWs with similar brain modular organization. The first-level analysis identified a range of 2 to 4 states for each region in more than 90% of subjects.

To reveal brain states that reoccurred across subjects and different levels of responsiveness, a second-level analysis was performed based on the individual-level brain states. First, for each subject and each condition, we averaged the inversed across-time MV_k of each region across TWs within each first-level brain state. The TWs of the largest averaged inversed across-time MV_k were labeled as 1, while the remaining TWs were labeled as 0. We then concatenated the TWs across all subjects and all conditions to generate a matrix, $iMV_{th}(n\times r)$, where n is the number of TWs multiplied by the number of subjects and conditions and r is the number of brain regions. Each column in the $iMV_{th}(n\times r)$ matrix represented whether a given brain region was temporally stable in its module in current TW. Finally, a similarity matrix, $S(n\times n)$, was computed as the inversed Euclidean distance between each pair of rows of $iMV_{th}(n\times r)$. We then performed a modularity analysis on $S(n\times n)$ to detect group-level brain states. Within each state, temporal stability was estimated as the proportion of 1 s in the matrix $iMV_{th}(n\times r)$.

2.11 | Statistical analysis

To detect differences in temporal stability between the two dominant states, a paired t test was performed ($p < .05$). To evaluate the spatial overlap between stable regions of each state and NCC areas, a nonparametric permutation test was used, whereby the ratio of NCC

members overlapping with stable regions (> mean) within each state was calculated. A total of 1000 random permutations were generated independently; for each permutation, stability values were randomly permuted across brain regions within each state, and the test statistic of interest was recalculated, generating a distribution of 1000 values from the permuted data. The p value was determined by comparing the observed value with the permutation-generated distribution. p values of less than .05 were considered statistically significant. To test which state involves more NCC members, we calculated the between-states difference in NCC overlapping ratio and performed the non-parametric permutation test using the same procedure as above.

To evaluate the effect of propofol-induced anesthesia, a one-way, repeated-measures ANOVA, with conscious condition (awake, sedation, and anesthesia) as the within-subject factor, was applied to measures of connectivity strength (NCC, feeder, and local connections) and modular variability (NCC and non-NCC members), respectively, followed by independent, post-hoc, paired t tests between every pair of conditions. Significance was considered at $p < .05$ and corrected for multiple comparisons using Bonferroni correction. Furthermore, network-based statistics (NBS) analysis was implemented using GRETNA MATLAB Toolbox (Wang et al., 2015) between pairs of conscious conditions, to reveal whole-brain network-based features of loss of consciousness with significance set at $p < .005$. Regional-wise comparisons of across-time MV between every pair of conditions were performed by paired t tests with significance set at $p < .05$ and corrected using False Discovery Rate (FDR) correction. The NBS and regional-wise results were presented using BrainNet Viewer (Xia et al., 2013).

2.12 | Validation analysis

To validate the reliability of anesthesia effects on FCS and MV of NCC, we randomly selected 10 subjects from the whole sample for 1000 times, and for each selected sub-samples, we performed one-way ANOVA to evaluate the effect of conscious level in static and dynamic FCS and MV of NCC. The ratio of significant ANOVA tests ($p < .05$) in FCS or MV was calculated as a measure of the reliability of anesthesia effects on NCC.

3 | RESULTS

3.1 | Rich-club structure of the functional brain network

Consistent with previous studies, we demonstrated that the functional brain network exhibited a significant rich-club structure compared to randomly reorganized networks for a range of connectivity strength $s = 1$ to $s = 30$ ($p < .001$, Figure S1). By displaying the anatomical distribution of rich-club members at different levels (top 10% to 50% connectivity strength, Figure 2a), we observed a tendency of a hierarchical layout for rich-club areas. While the primary sensorimotor, and auditory regions are among the lower level of connectivity strength (top 40%–50%), followed by association cortices of dorsolateral frontoparietal regions (top 20%–40%), the most highly-connected rich-club core (≥top 20%) is occupied by the anterior and posterior midline, bilateral temporoparietal junction areas, forming the default mode network (DMN). Note that regions in the occipital visual cortices also showed a high level of rich-clubness.

3.2 | Modular variability of the functional brain network

Modular analysis on the group-averaged functional brain networks revealed seven modules during the awake resting state (Figure S2), including the frontoparietal network (FPN), default mode network

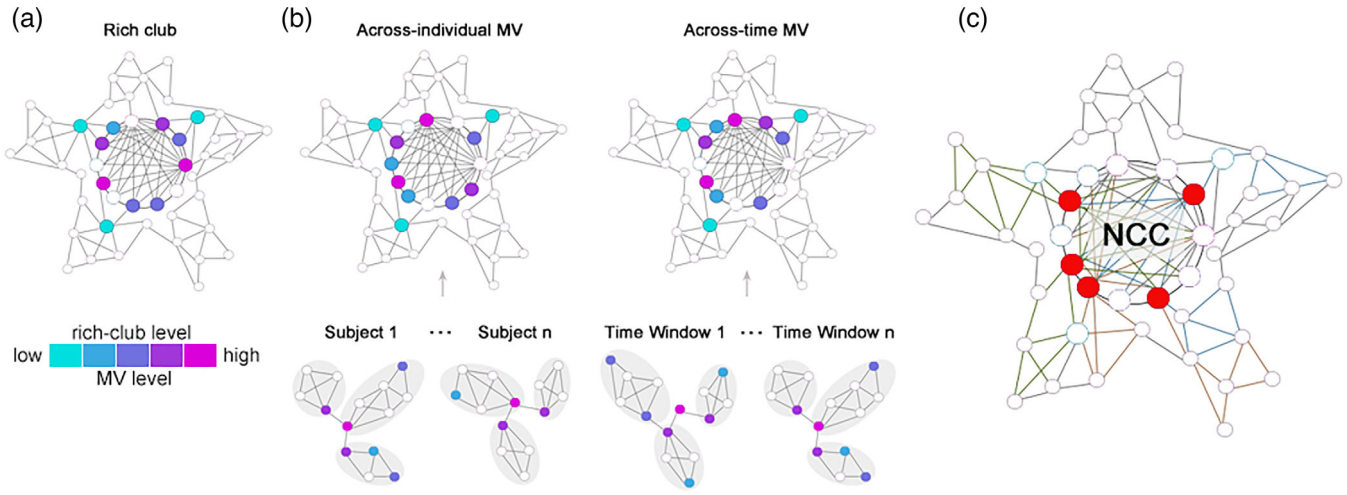

FIGURE 1 Schematic of the identification of neural correlates of consciousness (NCC). (a) Rich-club consists of high-degree hub regions that are more densely interconnected among themselves. (b) Brain regions that tend to sway between different modules across different subjects or different time windows are characterized by high across-individual or across-time modular variability. (c) Regions with high rich-club level, high across-individual MV as well as high across-time MV were overlapped to give rise to a putative NCC template

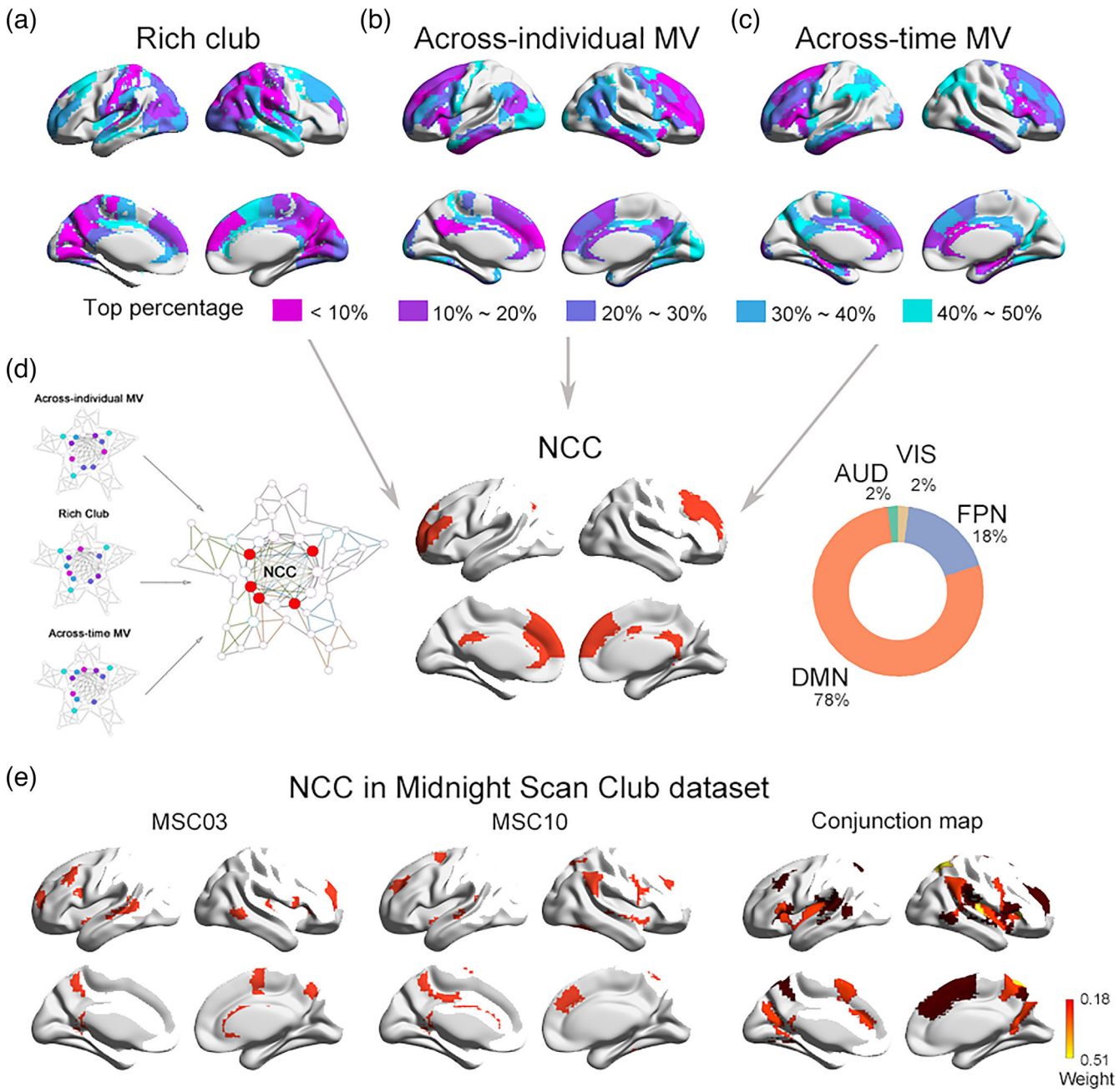

FIGURE 2 Neural correlates of consciousness (NCC) identification and functional decoding. (a–c) anatomical distribution of rich-club, across-individual MV, and across-time MV members at different levels (top 10% to 50%). (d) a putative NCC template by overlapping the three maps of regions with high rich-club connectedness (top 40%), high across-individual MV (top 40%), and high across-time MV (top 40%), 78% of which was in DMN and 18% was in FPN. (E) Individual-level GNW map for an example subject (MSC03) (upper) and the conjunction map of NCC map across individuals (lower) from the MSC data set

(DMN), auditory network (AUD), sensorimotor network (SMN), visual network (VIS), medial temporal lobe (MTL), and subcortical network. Figure 2b,c show the anatomical layout of brain regions with different levels of across-time and across-individual MV (top 10% to 50%). Regions in the frontal, temporoparietal, and insular cortices exhibit high variability in modular affiliation (≥top 20%), especially the medial and lateral prefrontal areas, which are among the highest in across-individual and across-time MV (top 10%).

3.3 | Identification of neural correlates of consciousness

By overlapping the above three maps (as shown in Figure 1) of regions with high rich-club connectedness (top 40%), high across-individual MV (top 40%), and high across-time MV (top 40%), we identified a putative NCC template of 20 brain areas (8% of all brain regions) distributing primarily in the anterior and posterior midline, lateral

prefrontal, and temporoparietal junction areas (Figure 2d). Remarkably, a large percent of these identified regions resided within the DMN (78%) and FPN (18%). We also generated overlapping maps of the three topological metrics using different percentiles (top 30% and top 50%) of regions with top rich-clubness and MV (Figure S3) and validated the robustness of the putative NCC candidates, especially the prefrontal regions that were consistently detected as potential NCC with both high interconnectivity and high modular variability. In addition, the identified NCC was found to mainly attributed to higher-order cognitive functions, and associated with genes enriched in synaptic transmission (see supplemental materials and Figure S4).

To further validate our findings, we replicated the NCC identification procedure above at the individual level using the MSC data set. Although there were variations across the individual-level NCC map (Figure S5), their conjunction map showed that the candidate NCC regions in more than 30% of subjects were predominately distributed in anterior, middle, and posterior cingulate cortices, middle frontal and temporoparietal cortices, and medial occipital gyrus (Figure 2E), which largely resembles the NCC distribution observed in our main data set.

3.4 | NCC candidates are more involved in a dynamically metastable state

The dynamical analysis identified five brain states at the group level. When projecting each brain state back to individuals, three states were presented in very few subjects and were thus discarded, resulting in two dominant brain states retained for further analysis. One of these two dominant brain states (state 1) exhibited higher stability than the other (state 2; Figure 3a left; $t = 12.05$, $p < 10^{-5}$), suggesting that brain state 1 may represent a temporally more stable state.

Figure 3b showed the brain regions with high stability (> mean) in each state. In state 1, we found that the most stable brain regions are preferentially distributed in the DMN and FPN modules, taking about 48% of all the stable regions (Figure 3c). In contrast, in state 2, the most stable regions were dominated by primary sensory and limbic networks (Figure 3b), with the DMN and FPN modules taking a less proportion (34% in total; Figure 3c right). By overlapping our identified NCC candidates with the stable regions in each state (Figure 3d), we observed that while both states exhibit significant overlaps with the NCC in regions of the prefrontal cortex, anterior and posterior cingulate cortices (*ps* <.001, permutation test), the stable regions in state 1 shared 13.64% with the NCC, which was significantly more ($p < .001$, permutation test) than that in state 2 (6.09%). We also evaluated the overlap between stable regions in each state with NCC candidates, identified at other rich-club and MV levels, and validated that the NCC overlapped more with stable regions in state 1 than in state 2 (Figure S6). Taking together, our results demonstrated that the spontaneous brain activities could be decomposed into a more stable brain state, steered predominately by the NCC members, and another less stable state dominated by primary sensorimotor regions which may be associated with subliminal processing.

3.5 | NCC signatures track loss of consciousness during propofol administration

Having identified the NCC and linked it with the metastable dynamic brain state, we next sought to investigate the role of the NCC in supporting human consciousness by comparing fMRI data in the same cohort of subjects from awake to sedation and unconscious state induced by different concentrations of the intravenous anesthetic

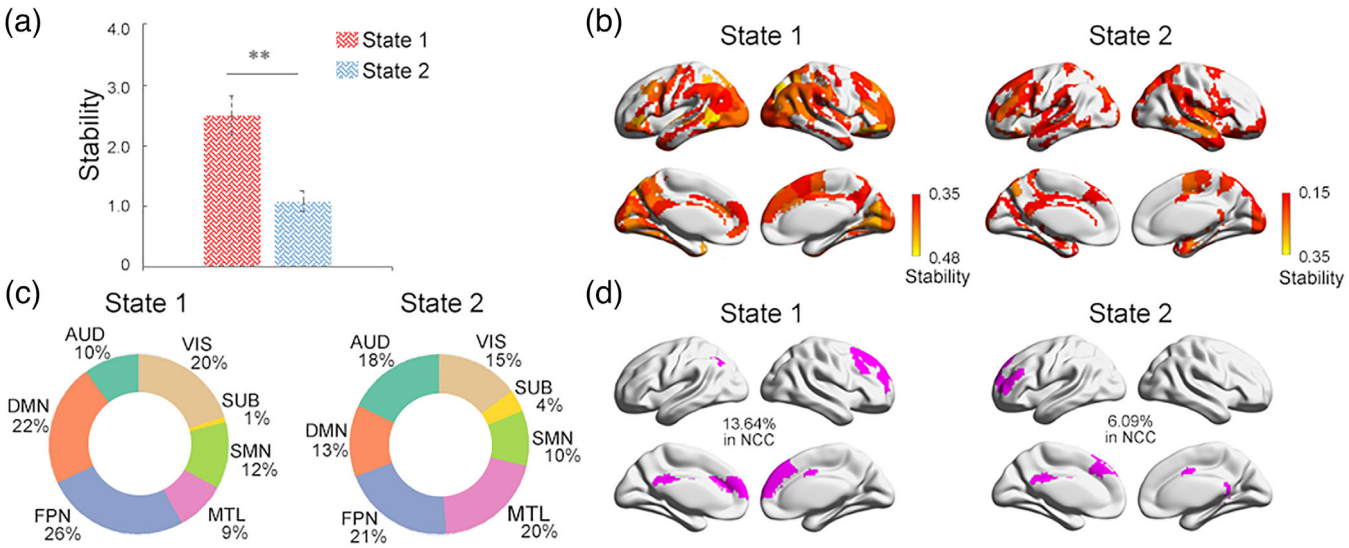

FIGURE 3 Neural correlates of consciousness (NCC) dynamics. (a) Two different iterating activity states with state 1 having higher stability than state 2. (b) Brain regions with high stability (>mean) and (c) their percentile distribution across brain modules in state 1 (left) and state 2 (right). (d) Overlaps between identified NCC space with the stable regions in state 1 (left) and state 2 (right)

propofol. The identification of NCC allowed for the classification of brain regions as NCC and non-NCC members, and connections into three categories, including NCC connections linking NCC members, feeder connections linking NCC and non-NCC regions, and local connections linking non-NCC regions. We, therefore, calculated MV for NCC and non-NCC regions, and FC strength (FCS) for the three categories of connections, respectively, and expected to observe alterations, especially within the NCC, during the anesthesia-induced loss of consciousness.

One-way ANOVA revealed marginally significant effects of anesthesia in static FC strength (Figure 4A) of local connections (F [2,26] = 3.59, $p_{uncorrected}$ = .04, $p_{uncorrected}$ = .12), and marginally significant effect of anesthesia in NCC connections (F [2,26] = 3.57, $p_{uncorrected}$ = .04, $p_{uncorrected}$ = .12), both of which decreased with loss of consciousness. Post-hoc tests found no significant changes in NCC or local connections between each pair of the three conscious levels. To further explore which specific connections are impacted during propofol administration, we performed network-based statistics (NBS) between different conscious levels for NCC and local connections respectively. Our results for NCC connections revealed significant decreases in the strength of FC among the midline key regions of the DMN, including the medial prefrontal cortex (mPFC), anterior cingulate cortex (ACC), and posterior cingulate cortex (PCC), between wakefulness and anesthesia (p < .005), and among the midline DMN areas and lateral middle frontal gyrus (MFG) between sedation and anesthesia (p < .005, Figure 4c). As for the local connections (Figure S7), reductions in FC were mainly distributed among SMN, VIS, and MTL networks (p < .005).

We also observed marginally significant effects of loss of consciousness in across-time MV only within the NCC (F [2,26] = 3.76, $p_{uncorrected}$ = .037, $p_{corrected}$ = .074), with the across-time MV decreased as the dose of anesthesia deepened (Figure 4b). Post-hoc tests found no significant changes between pairs of the three conscious levels. Further regional-wise paired t comparisons revealed significant reductions of across-time MV located primarily in the medial and lateral prefrontal areas from sedation to anesthesia ($p_{corrected}$ <.05, Figure 4c), indicating the evident degeneration of the ability for these regions to dynamically vary their modular affiliation across time. No significant effect of consciousness was found in across-individual MV.

Dynamic analysis of brain states revealed that significant anesthesia-related changes in FC strength were observed only during the stable state (state 1) within the NCC (F [2,23] = 7.59, $p_{uncorrected}$ = .003, $p_{corrected}$ = .009, Figure 5a). Marginally significant effect of anesthesia was also observed for feeder (F [2,23] = 3.84, $p_{uncorrected}$ = .038, $p_{corrected}$ = .11) and local connections (F [2,23] = 3.77, $p_{uncorrected}$ = .040, $p_{corrected}$ = .12) during the stable state. Post-hoc tests revealed significant decreases in NCC connectivity from sedation to anesthesia (t = 4.37, $p_{uncorrected}$ = .001, $p_{corrected}$ = .003) during the stable state, while no significant between-condition differences were observed for feeder or local connections. Further NBS analysis of NCC connections in state 1 revealed significant decreases among regions of mPFC, ACC, PCC, and MFG (p < .005, Figure 5b). As for the feeder connections, significant reductions were mostly between NCC regions with non-NCC regions in DMN from awake to anesthesia, and with non-NCC regions in FPN from sedation

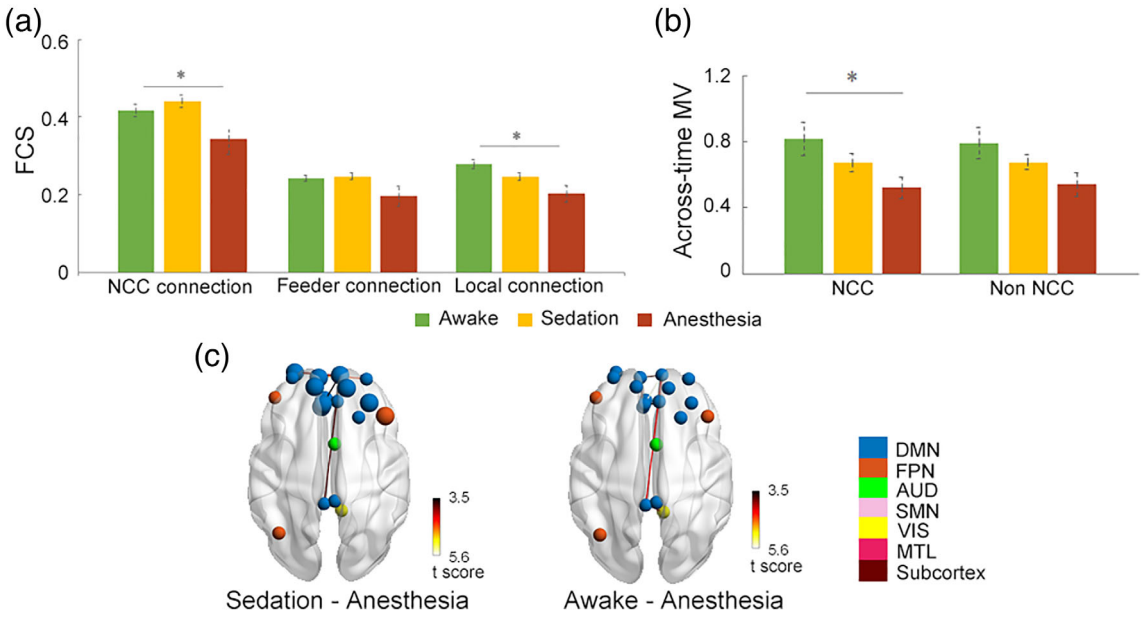

FIGURE 4 Static NCC signatures track loss of consciousness during Propofol anesthesia. (a) Differences in static FC of NCC, feeder, and local connections from awake to sedation and unconsciousness. (b) Differences in across-time MV of NCC and non-NCC regions from awake to sedation and unconsciousness. (c) NCC connections show significant reductions in NBS between awake and unconsciousness, and NCC regions with significant decreases in across-time MV from sedation to anesthesia condition (highlighted in larger circles). The color of nodes indicates modular affiliation. *$p_{uncorrected}$ < .05

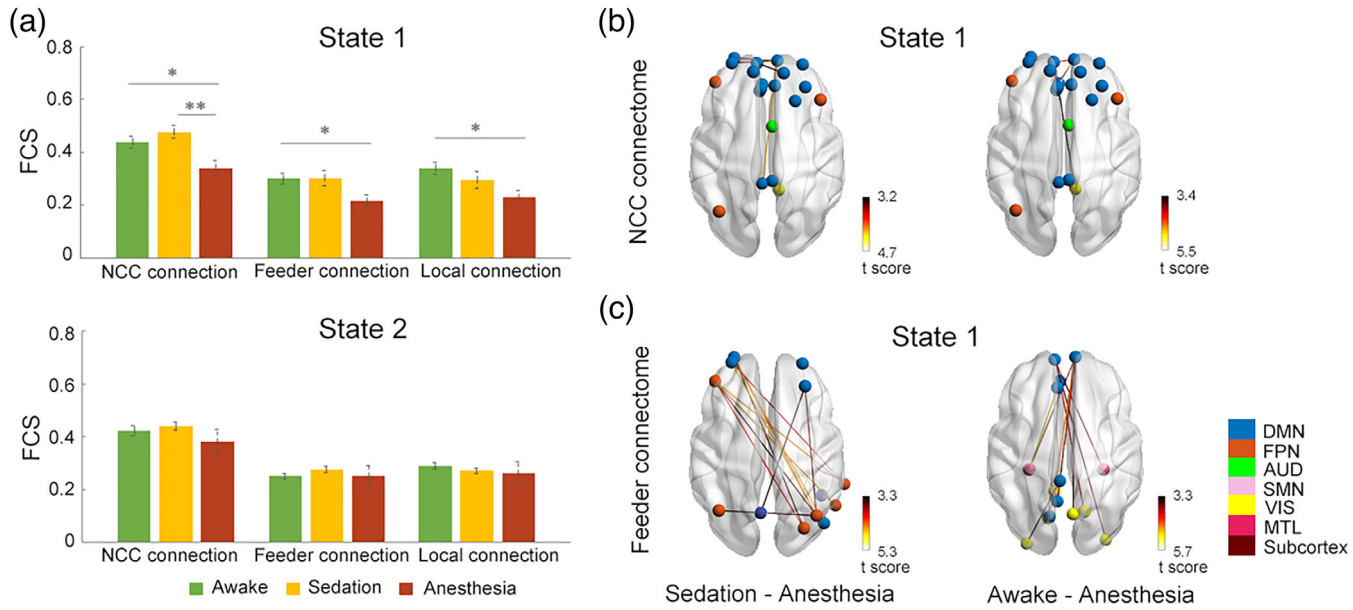

FIGURE 5 Dynamic NCC signatures track loss of consciousness during Propofol anesthesia. (a) Differences in dynamic FC of NCC, feeder, and local connections from awake to sedation and unconsciousness during each state. (b) NCC connections show significant reductions in NBS between different conscious levels during state 1. (c) Feeder connections show significant reductions in NBS between different conscious levels during state 1. The color of nodes indicates modular affiliation. $^{*}p_{\text{uncorrected}} < .05$; $^{**}p_{\text{corrected}} < .05$

to anesthesia ($p < .005$, Figure 5b). Local connections among a cluster of regions across the posterior part of the brain were shown to reduce from awake and sedation to anesthesia ($p < .005$, Figure S7). No significant effect of anesthesia was observed in across-time MV in either of the two dynamic states. Similar anesthesia effects were also observed using the NCC identified at different rich-club and MV levels (Figure S8).

Validation analyses further showed that NCC regions were significantly modulated by loss of consciousness. For static analysis, there is a consistent effect of conscious level in NCC connectivity in 57% of sub-samples, and in MV in 31% of sub-samples. During dynamic state 1, in which NCC candidates have been demonstrated to be more involved, the significant effect of the conscious level was reliably observed in NCC connectivity in 83% of sub-samples. In contrast, during state 2, a significant effect in NCC connectivity was only observed in about 18% of sub-samples.

4 | DISCUSSION

The present study proposes to locate the neural correlates of consciousness by taking advantage of recent developments in network neuroscience. We identified a cluster of regions distributed in prefrontal and temporoparietal cortices that are characterized by both high functional interconnectivity and high modular variability to constitute the putative NCC. Dynamic analysis revealed two discrete reoccurring brain states, which are characterized by their differences in temporal stability—the state dominated by the identified NCC appears to be temporally more stable than the other state predominately composed of primary regions, demonstrating that the identified neural correlates of consciousness are able to sustain conscious contents as metastable network representations. Finally, we showed that the identified NCC candidates were significantly modulated in terms of functional connectedness and modular variability in response to the loss of consciousness during propofol anesthesia.

Combing two well-defined graph-theoretical network measures, we located the putative NCC members in a distributed set of regions residing predominately in the default-mode and frontoparietal networks. While the identified regions included the posterior cingulate and temporoparietal cortices, which are the main candidates for the "posterior hot zones" advocated by the IIT, the inclusion of anterior areas in the putative NCC provides support for the GNW theory. Notably, regions in the anterior cortex were observed to show both the densest connectivity and the highest modular variability, situating at the core of the putative NCC. This is in well concordance with initial theoretical and simulation studies of GNW predicting the dorsolateral prefrontal and anterior cingulate cortices to be the major contributors to the workspace (Dehaene et al., 1998), and is also consistent with recent efforts in quantifying the global workspace (Deco et al., 2021; Luppi et al., 2020) by considering the brain as an information processing system. The posterior cortical regions, on the other hand, were of high connectivity but relatively low temporal variability in modular structures. This is in line with a recent study(Luppi et al., 2020) demonstrating that the default mode system, especially its posterior regions, exhibited a higher prevalence of synergistic over redundant information, which suggests an integrating rather than broadcasting role of these regions in processing information accessible to consciousness. Thus, the PCC may act as an integrator with rich

connections, gathering information from distributed brain networks as the GNW theory has postulated, but may be less responsible for information differentiation in terms of spatiotemporal variability in the brain modules, failing to provide strong support for the IIT. We note that GNWT and IIT are only two examples of the many theories of consciousness, there are other theories, such as the Higher-order Thought Theory (HOT), Recurrent Processing Theory (RPT), and Synchrony Theory (ST), also make predictions for the neural locus of consciousness. Similar to the divide between GNWT and IIT, these theories also diverge in considering either the sensory regions (RPT and ST) or the prefrontal cortex (HOT) to be sufficient for consciousness. Our findings of the widespread distribution of NCC candidates point to a more global, integrated substrate of consciousness that may contribute to the ongoing discussion(Ihalainen et al., 2021; Koch et al., 2016).

Notably, our proposed analytic framework, leveraging graph-theoretical tools to locate the NCC architecture, highlights the importance of characterizing the spatio-temporal features of the brain in understanding consciousness, which seems to fit well with the TTC theory. The TTC proposes that the key to consciousness lies in the topography and temporal dynamics of brain activity (Northoff & Huang, 2017; Northoff & Lamme, 2020; Northoff & Zilio, 2022a, 2022b). Especially, the TTC postulates four different neuronal mechanisms accounting for the different dimensions of consciousness, of which the "temporo-spatial nestedness" of the spontaneous activity accounting for the level/state of consciousness may be particularly relevant to our results obtained using resting-state data. The level/state of consciousness is considered a global signature that integrates intrinsic neural activities across different temporal and spatial scales (Northoff & Zilio, 2022b). As such, the spatial organization and temporal dynamics that balance between integration and segregation of spontaneous brain activity are proposed to be central to understanding the neural correlates of consciousness (Northoff & Zilio, 2022b). Previous studies have reported non-trivial properties, including centrality and modularity (Barttfeld et al., 2015; Betzel et al., 2016; He et al., 2009; Meunier et al., 2010), as well as a rich dynamic repertoire of spontaneous brain activity (Barttfeld et al., 2015; Betzel et al., 2016; Cavanna et al., 2018; Li et al., 2020; Liu et al., 2018; Raut et al., 2020; Shine & Poldrack, 2018), demonstrating the "temporo-spatial nestedness" of the intrinsic brain organization. In consistent with these theoretical and empirical evidence, our analyses complement the understanding of the anatomical footprints underlying consciousness by demonstrating their superior ability not only in functional integration but also in dynamic functional diversification with specialized modular processors.

Our observations from dynamic analysis provide further evidence supporting the functional implications of the NCC architecture in the temporal domain. Despite the disagreement among the GNWT, IIT, TTC, and other theories of consciousness, they all seem to either explicitly or implicitly agree that consciousness is closely related to the transition from segregated to integrated neural activity, which is supposed to lead to stable, synchronous states embedded in the temporo-spatial dynamics of consciousness (Northoff & Lamme, 2020). Specially, based on theoretical and simulation evidence, the GNW theory predicts two dynamic states or stages for a stimulus to access consciousness (Dehaene & Changeux, 2011): an "ignited" conscious state when the input signal is strong enough to ignite a sustained, metastable distributed neural representation of the current conscious contents; and a subliminal processing state during which the incoming activity is propagated through primary sensory areas, inducing only a progressively decaying activity in higher-order regions. Intriguingly, this fits well with the roles that our findings assigned to the two brain states identified herein. Specifically, we demonstrated that within the brain state of higher temporal stability of modular organization, a significant percentage of the most stable regions coincide with the identified NCC. In contrast, the other brain state showing significantly lower stability is mainly steered by primary sensory areas. Furthermore, our results pinpoint the default midline areas to be the temporally most stable sites during the temporally more stable state, which refines our understanding of the critical value of DMN areas in maintaining neural representations that access consciousness. This observation is also consistent with recent studies showing that the default mode regions that are distant from sensory input have the longest timescale to accumulate and process information, which may facilitate functional integration over a slow timescale (Baldassano et al., 2017; Chien & Honey, 2020; Raut et al., 2020).

In supportive of NCC's roles in human consciousness, we demonstrated their selective vulnerability during anesthesia-induced loss of consciousness. During the loss of consciousness, although static FC strength of both NCC and local connections decreased, the dynamic analysis revealed that connectivity within the NCC was particularly impacted during the temporally more stable state, which is consistent with previous dynamic connectivity studies in patients under pharmacological or pathological unconsciousness, showing more extensively disruptions in states that potentially relevant for conscious processing (Barttfeld et al., 2015; Demertzi et al., 2019; Luppi et al., 2019). Furthermore, we also found that the identified NCC members exhibited different anesthesia-related changing patterns in terms of the two network measures, FCS and MV. Specifically, FCS reductions were specific to the DMN midline areas, while decreases in MV were observed predominately in prefrontal cortices, suggesting that these two sets of regions within the NCC may play complementary roles in supporting consciousness. This observation is in line with the previous hypothesis proposing that the areas constituting the neural substrates supporting consciousness are "neither identical nor redundant" (Mashour et al., 2020), and offers novel insight into the understanding of functional specificity of NCC members. The FCS indicates a region's ability in integrating or amplifying segregated information, while the temporal modular variability reflects its temporal flexibility in selecting or broadcasting information with a wide range of local processors. Thus, the DMN midline regions may be well-suited for functional integration rather than functional diversification, while the prefrontal areas may function distinctly in support of conscious processing. Indeed, recent insights from connectivity decomposition analysis found that the DMN is situated at the top of the topographical hierarchy in brain connectivity space, supporting its essential role in

acting as cortical hubs with a maximal distance from primary systems to integrate and represent multi-dimensional information (Margulies et al., 2016). In contrast, the fronto-parietal system was found to occupy a position sitting between the unimodal and default mode networks, suggesting it may function as a connector to collect bottom-up information and distribute top-down information (Margulies et al., 2016). Notably, the medial prefrontal region exhibited reduction in both FCS and temporal MV associated with propofol anesthesia, indicating a crucial role of this anterior cluster in contributing to conscious experience. Taking together, these observations provide evidence for the pivotal contribution of the identified putative NCC, which covered most key structures predicted by both GNW and IIT, in supporting human consciousness, and more importantly, highlight the potential differential roles between prefrontal GNW regions and posterior IIT regions during propofol-induced loss of consciousness (Ihalainen et al., 2021).

5 | LIMITATION

There are a few limitations to note in our study. First, given the relatively limited scan duration of our primary data set (8 mins), NCC identification was only performed at group-level, which would underestimate potential individual differences in the topography and topology of the NCC architecture. To mitigate this concern, we conducted an individualized analysis on the MSC data set and validated that the individual-level NCC distribution was similar to that on the group level. Nevertheless, future research would benefit to consider constructing individualized NCC to predict between-subject variability in conscious access and related cognitive abilities. Second, we used a single type of anesthetic (a $GABA_A$ receptor agonist) to induce loss of consciousness. It is unknown whether our observation of the disruptions during propofol-induced anesthesia could generalize to other types of anesthetics or other forms of unconsciousness. Previous studies have consistently related changes in the prefrontal and default mode regions, which are key members of the NCC identified herein, to unconsciousness induced by various types of anesthetic or disorders of consciousness (Alkire et al., 2008; Chuang & Nasrallah, 2017; Huang et al., 2020; Lee et al., 2013), attesting to the generality of NCC's selective vulnerability. However, NCC members could still exhibit different spatiotemporal changing patterns during different forms of unconsciousness, which warrants future investigations. Third, NCC was only probed based on resting-state fMRI data, it would be interesting to extend the current analytic framework to task data in future studies, which may help to understand how the putative NCC would be modulated by varied conscious contents during task stimulus.

6 | CONCLUSION

The present findings testify to the NCC's abilities in information integration and differentiation and provide novel insights into reconciling the ongoing discussion of the contribution of anterior versus posterior regions in supporting human consciousness.

ACKNOWLEDGMENTS

This work was supported by the National Natural Science Foundation of China (https://www.nsfc.gov.cn/, grant numbers 82072000 and 81671769 to [XL]); the Central University Basic Research Fund of China (https://www.edu.cn/, grant number HIT. NSRIF. 2020042 to [XL]); the Natural Science Foundation of Heilongjiang Province, China (http://kjt.hlj.gov.cn/, grant number LH2019H001 to [XL]); and National Natural Science Foundation of China (https://www.nsfc.gov.cn/, grant number 82171261 to [JZ]).

CONFLICT OF INTEREST

The authors have declared that no competing interests exist.

DATA AVAILABILITY STATEMENT

The data under propofol administration that support the findings of this study are not publicly available due to restrictions imposed by the administering institution and the privacy of participants. The authors will share them by request from any qualified investigator after completion of a data sharing agreement. The MSC data is a publically available dataset at Midnight Scan Club website (https://legacy.openfmri.org/dataset/ds000224/).

CODE AVAILABILITY STATEMENT

Code for data cleaning and analysis will be updated as part of the replication package once the paper has been conditionally accepted.

ORCID

Siyang Li https://orcid.org/0000-0002-3730-2171

REFERENCES

Alkire, M. T., Hudetz, A. G., & Tononi, G. (2008). Consciousness and anesthesia. *Science*, *322*(5903), 876–880.

Allen, E. A., Damaraju, E., Plis, S. M., Erhardt, E. B., Eichele, T., & Calhoun, V. D. (2014). Tracking whole-brain connectivity dynamics in the resting state. *Cerebral Cortex*, *24*(3), 663–676.

Baldassano, C., Chen, J., Zadbood, A., Pillow, J. W., Hasson, U., & Norman, K. A. (2017). Discovering event structure in continuous narrative perception and memory. *Neuron*, *95*(3), 709–721 e705.

Barttfeld, P., Uhrig, L., Sitt, J. D., Sigman, M., Jarraya, B., & Dehaene, S. (2015). Signature of consciousness in the dynamics of resting-state brain activity. *Proceedings of the National Academy of Sciences of the United States of America*, *112*(3), 887–892.

Betzel, R. F., Fukushima, M., He, Y., Zuo, X. N., & Sporns, O. (2016). Dynamic fluctuations coincide with periods of high and low modularity in resting-state functional brain networks. *NeuroImage*, *127*, 287–297.

Blondel, V. D., Guillaume, J. L., Lambiotte, R., & Lefebvre, E. (2008). Fast unfolding of communities in large networks. *Journal of Statistical Mechanics-Theory and Experiment*, *10*, P10008.

Boly, M., Faymonville, M. E., Schnakers, C., Peigneux, P., Lambermont, B., Phillips, C., Lancellotti, P., Luxen, A., Lamy, M., Moonen, G., Maquet, P., & Laureys, S. (2008). Perception of pain in the minimally conscious state with PET activation: An observational study. *Lancet Neurology*, *7*(11), 1013–1020.

Boly, M., Massimini, M., Tsuchiya, N., Postle, B. R., Koch, C., & Tononi, G. (2017). Are the neural correlates of consciousness in the front or in the Back of the cerebral cortex? Clinical and neuroimaging evidence. *Journal of Neuroscience*, *37*(40), 9603–9613.

Boveroux, P., Vanhaudenhuyse, A., Bruno, M. A., Noirhomme, Q., Lauwick, S., Luxen, A., Degueldre, C., Plenevaux, A., Schnakers, C., Phillips, C., Brichant, J. F., Bonhomme, V., Maquet, P., Greicius, M. D., Laureys, S., & Boly, M. (2010). Breakdown of within- and between-network resting state functional magnetic resonance imaging connectivity during Propofol-induced loss of consciousness. *Anesthesiology*, *113*(5), 1038–1053.

Brown, R., Lau, H., & LeDoux, J. E. (2019). Understanding the higher-order approach to consciousness. *Trends in Cognitive Sciences*, *23*(9), 754–768.

Cavanna, F., Vilas, M. G., Palmucci, M., & Tagliazucchi, E. (2018). Dynamic functional connectivity and brain metastability during altered states of consciousness. *NeuroImage*, *180*(Pt B), 383–395.

Chien, H. Y. S., & Honey, C. J. (2020). Constructing and forgetting temporal context in the human cerebral cortex. *Neuron*, *106*(4), 675.

Chuang, K. H., & Nasrallah, F. A. (2017). Functional networks and network perturbations in rodents. *NeuroImage*, *163*, 419–436.

Cohen, J. R., & D'Esposito, M. (2016). The segregation and integration of distinct brain networks and their relationship to cognition. *Journal of Neuroscience*, *36*(48), 12083–12094.

Colizza, V., Flammini, A., Serrano, M. A., & Vespignani, A. (2006). Detecting rich-club ordering in complex networks. *Nature Physics*, *2*(2), 110–115.

Cox, R. W. (1996). AFNI: Software for analysis and visualization of functional magnetic resonance neuroimages. *Computers and Biomedical Research*, *29*(3), 162–173.

Cribben, I., Haraldsdottir, R., Atlas, L. Y., Wager, T. D., & Lindquist, M. A. (2012). Dynamic connectivity regression: Determining state-related changes in brain connectivity. *NeuroImage*, *61*(4), 907–920.

Cui, Z., Li, H., Xia, C. H., Larsen, B., Adebimpe, A., Baum, G. L., Cieslak, M., Gur, R. E., Gur, R. C., Moore, T. M., Oathes, D. J., Alexander-Bloch, A. F., Raznahan, A., Roalf, D. R., Shinohara, R. T., Wolf, D. H., Davatzikos, C., Bassett, D. S., Fair, D. A., … Satterthwaite, T. D. (2020). Individual variation in functional topography of association networks in youth. *Neuron*, *106*(2), 340–353 e348.

Deco, G., Vidaurre, D., & Kringelbach, M. L. (2021). Revisiting the global workspace orchestrating the hierarchical organization of the human brain. *Nature Human Behaviour*, *5*(4), 497–511.

Dehaene, S., & Changeux, J. P. (2011). Experimental and theoretical approaches to conscious processing. *Neuron*, *70*(2), 200–227.

Dehaene, S., Changeux, J.-P., & Naccache, L. (2011). The global neuronal workspace model of conscious access: From neuronal architectures to clinical applications. In *Characterizing Consciousness: From Cognition to the Clinic?* (pp. 55–84). Springer-Verlag Berlin Heidelberg. https://doi.org/10.1007/978-3-642-18015-6_4

Dehaene, S., Kerszberg, M., & Changeux, J. P. (1998). A neuronal model of a global workspace in effortful cognitive tasks. *Proceedings of the National Academy of Sciences of the United States of America*, *95*(24), 14529–14534.

Demertzi, A., Tagliazucchi, E., Dehaene, S., Deco, G., Barttfeld, P., Raimondo, F., Martial, C., Fernandez-Espejo, D., Rohaut, B., Voss, H. U., Schiff, N. D., Owen, A. M., Laureys, S., Naccache, L., & Sitt, J. D. (2019). Human consciousness is supported by dynamic complex patterns of brain signal coordination. *Science Advances*, *5*(2), eaat7603.

Fan, L. Z., Li, H., Zhuo, J. J., Zhang, Y., Wang, J. J., Chen, L. F., Yang, Z. Y., Chu, C. Y., Xie, S. M., Laird, A. R., Fox, P. T., Eickhoff, S. B., Yu, C. S., & Jiang, T. Z. (2016). The human Brainnetome Atlas: A new brain Atlas based on connectional architecture. *Cerebral Cortex*, *26*(8), 3508–3526.

Gordon, E. M., Laumann, T. O., Gilmore, A. W., Newbold, D. J., Greene, D. J., Berg, J. J., Ortega, M., Hoyt-Drazen, C., Gratton, C., Sun, H., Hampton, J. M., Coalson, R. S., Nguyen, A. L., McDermott, K. B., Shimony, J. S., Snyder, A. Z., Schlaggar, B. L., Petersen, S. E., Nelson, S. M., & Dosenbach, N. U. F. (2017). Precision functional mapping of individual human brains. *Neuron*, *95*(4), 791–807 e797.

Hawrylycz, M., Miller, J. A., Menon, V., Feng, D., Dolbeare, T., Guillozet-Bongaarts, A. L., Jegga, A. G., Aronow, B. J., Lee, C. K., Bernard, A., Glasser, M. F., Dierker, D. L., Menche, J., Szafer, A., Collman, F., Grange, P., Berman, K. A., Mihalas, S., Yao, Z. Z., … Lein, E. (2015). Canonical genetic signatures of the adult human brain. *Nature Neuroscience*, *18*(12), 1832–1844.

He, Y., Lim, S., Fortunato, S., Sporns, O., Zhang, L., Qiu, J., Xie, P., & Zuo, X. N. (2018). Reconfiguration of cortical networks in MDD uncovered by multiscale community detection with fMRI. *Cerebral Cortex*, *28*(4), 1383–1395.

He, Y., Wang, J., Wang, L., Chen, Z. J., Yan, C., Yang, H., Tang, H., Zhu, C., Gong, Q., Zang, Y., & Evans, A. C. (2009). Uncovering intrinsic modular organization of spontaneous brain activity in humans. *PLoS One*, *4*(4), e5226.

Huang, Z., Zhang, J., Wu, J., Liu, X., Xu, J., Zhang, J., Qin, P., Dai, R., Yang, Z., Mao, Y., Hudetz, A. G., & Northoff, G. (2018). Disrupted neural variability during propofol-induced sedation and unconsciousness. *Human Brain Mapping*, *39*(11), 4533–4544.

Huang, Z. R., Zhang, J., Wu, J. S., Mashour, G. A., & Hudetz, A. G. (2020). Temporal circuit of macroscale dynamic brain activity supports human consciousness. *Science Advances*, *6*(11), eaaz0087.

Ihalainen, R., Gosseries, O., de Steen, F. V., Raimondo, F., Panda, R., Bonhomme, V., Marinazzo, D., Bowman, H., Laureys, S., & Chennu, S. (2021). How hot is the hot zone? Computational modelling clarifies the role of parietal and frontoparietal connectivity during anaesthetic-induced loss of consciousness. *NeuroImage*, *231*, 117841.

Koch, C., Massimini, M., Boly, M., & Tononi, G. (2016). Posterior and anterior cortex - where is the difference that makes the difference? *Nature Reviews. Neuroscience*, *17*(10), 666.

Laureys, S., Antoine, S., Boly, M., Elincx, S., Faymonville, M. E., Berre, J., Sadzot, B., Ferring, M., De Tiege, X., van Bogaert, P., Hansen, I., Damas, P., Mavroudakis, N., Lambermont, B., Del Fiore, G., Aerts, J., Degueldre, C., Phillips, C., Franck, G., … Maquet, P. (2002). Brain function in the vegetative state. *Acta Neurologica Belgica*, *102*(4), 176–185.

Lee, U., Ku, S., Noh, G., Baek, S., Choi, B., & Mashour, G. A. (2013). Disruption of frontal-parietal communication by ketamine, Propofol, and Sevoflurane. *Anesthesiology*, *118*(6), 1264–1275.

Lee, U., & Mashour, G. A. (2018). Role of network science in the study of anesthetic state transitions. *Anesthesiology*, *129*(5), 1029–1044.

Li, L., Lu, B., & Yan, C. G. (2020). Stability of dynamic functional architecture differs between brain networks and states. *NeuroImage*, *216*, 116230.

Li, M., Wang, D., Ren, J., Langs, G., Stoecklein, S., Brennan, B. P., Lu, J., Chen, H., & Liu, H. (2019). Performing group-level functional image analyses based on homologous functional regions mapped in individuals. *PLoS Biology*, *17*(3), e2007032.

Liao, X., Cao, M., Xia, M., & He, Y. (2017). Individual differences and time-varying features of modular brain architecture. *NeuroImage*, *152*, 94–107.

Liu, X., Zhang, N., Chang, C., & Duyn, J. H. (2018). Co-activation patterns in resting-state fMRI signals. *NeuroImage*, *180*(Pt B), 485–494.

Luppi, A. I., Craig, M. M., Pappas, I., Finoia, P., Williams, G. B., Allanson, J., Pickard, J. D., Owen, A. M., Naci, L., Menon, D. K., & Stamatakis, E. A. (2019). Consciousness-specific dynamic interactions of brain integration and functional diversity. *Nature Communications*, *10*(1), 4616.

Luppi, A. I., Mediano, P. A. M., Rosas, F. E., Allanson, J., Pickard, J. D., Carhart-Harris, R. L., Williams, G. B., Craig, M. M., Finoia, P., Owen, A. M., Naci, L., Menon, D. K., Bor, D., & Stamatakis, E. A. (2020). A synergistic workspace for human consciousness revealed by integrated information decomposition. *BioRxiv*. https://doi.org/10.1101/2020.11.25.398081

Margulies, D. S., Ghosh, S. S., Goulas, A., Falkiewicz, M., Huntenburg, J. M., Langs, G., Bezgin, G., Eickhoff, S. B., Castellanos, F. X., Petrides, M., Jefferies, E., & Smallwood, J. (2016). Situating the default-mode network along a principal gradient of macroscale cortical organization. *Proceedings of the National Academy of Sciences of the United States of America*, *113*(44), 12574–12579.

Marsh, B., White, M., Morton, N., & Kenny, G. N. (1991). Pharmacokinetic model driven infusion of propofol in children. *British Journal of Anaesthesia*, *67*(1), 41–48.

Mashour, G. A. (2018). The controversial correlates of consciousness new data suggest that the prefrontal cortex ignites networks supporting consciousness. *Science*, *360*(6388), 493–494.

Mashour, G. A., Roelfsema, P., Changeux, J. P., & Dehaene, S. (2020). Conscious processing and the global neuronal workspace hypothesis. *Neuron*, *105*(5), 776–798.

Melloni, L., Mudrik, L., Pitts, M., & Koch, C. (2021). Making the hard problem of consciousness easier. *Science*, *372*(6545), 911–912.

Meunier, D., Lambiotte, R., & Bullmore, E. T. (2010). Modular and hierarchically modular organization of brain networks. *Frontiers in Neuroscience*, *4*, 200.

Mhuircheartaigh, R. N., Rosenorn-Lanng, D., Wise, R., Jbabdi, S., Rogers, R., & Tracey, I. (2010). Cortical and subcortical connectivity changes during decreasing levels of consciousness in humans: A functional magnetic resonance imaging study using Propofol. *Journal of Neuroscience*, *30*(27), 9095–9102.

Newman, M. E. J., & Girvan, M. (2004). Finding and evaluating community structure in networks. *Physical Review E*, *69*(2), 026113.

Northoff, G., & Huang, Z. (2017). How do the brain's time and space mediate consciousness and its different dimensions? Temporo-spatial theory of consciousness (TTC). *Neuroscience and Biobehavioral Reviews*, *80*, 630–645.

Northoff, G., & Lamme, V. (2020). Neural signs and mechanisms of consciousness: Is there a potential convergence of theories of consciousness in sight? *Neuroscience and Biobehavioral Reviews*, *118*, 568–587.

Northoff, G., & Zilio, F. (2022a). From shorter to longer timescales: Converging integrated information theory (IIT) with the Temporo-spatial theory of consciousness (TTC). *Entropy (Basel)*, *24*(2), 270.

Northoff, G., & Zilio, F. (2022b). Temporo-spatial theory of consciousness (TTC) - bridging the gap of neuronal activity and phenomenal states. *Behavioural Brain Research*, *424*, 113788.

Odegaard, B., Knight, R. T., & Lau, H. (2017). Should a few null findings falsify prefrontal theories of conscious perception? *Journal of Neuroscience*, *37*(40), 9593–9602.

Oizumi, M., Albantakis, L., & Tononi, G. (2014). From the phenomenology to the mechanisms of consciousness: Integrated information theory 3.0. *PLoS Computational Biology*, *10*(5), e1003588.

Opsahl, T., Colizza, V., Panzarasa, P., & Ramasco, J. J. (2008). Prominence and control: The weighted Rich-Club effect. *Physical Review Letters*, *101*(16), 168702.

Power, J. D., Barnes, K. A., Snyder, A. Z., Schlaggar, B. L., & Petersen, S. E. (2012). Spurious but systematic correlations in functional connectivity MRI networks arise from subject motion. *NeuroImage*, *59*(3), 2142–2154.

Power, J. D., Cohen, A. L., Nelson, S. M., Wig, G. S., Barnes, K. A., Church, J. A., Vogel, A. C., Laumann, T. O., Miezin, F. M., Schlaggar, B. L., & Petersen, S. E. (2011). Functional network Organization of the Human Brain. *Neuron*, *72*(4), 665–678.

Ramsay, M. A., Savege, T. M., Simpson, B. R., & Goodwin, R. (1974). Controlled sedation with alphaxalone-alphadolone. *British Medical Journal*, *2*(5920), 656–659.

Raut, R. V., Snyder, A. Z., & Raichle, M. E. (2020). Hierarchical dynamics as a macroscopic organizing principle of the human brain. *Proceedings of the National Academy of Sciences of the United States of America*, *117*(34), 20890–20897.

Rubinov, M., & Sporns, O. (2011). Weight-conserving characterization of complex functional brain networks. *NeuroImage*, *56*(4), 2068–2079.

Schrouff, J., Perlbarg, V., Boly, M., Marrelec, G., Boveroux, P., Vanhaudenhuyse, A., Bruno, M. A., Laureys, S., Phillips, C., Pelegrini-Issac, M., Maquet, P., & Benali, H. (2011). Brain functional integration decreases during propofol-induced loss of consciousness. *NeuroImage*, *57*(1), 198–205.

Shine, J. M., & Poldrack, R. A. (2018). Principles of dynamic network reconfiguration across diverse brain states. *NeuroImage*, *180*(Pt B), 396–405.

Sporns, O., & Betzel, R. F. (2016). Modular brain networks. *Annual Review of Psychology*, *67*(67), 613–640.

Steen, M., Hayasaka, S., Joyce, K., & Laurienti, P. (2011). Assessing the consistency of community structure in complex networks. *Physical Review E*, *84*(1), 016111.

Tanabe, S., Huang, Z., Zhang, J., Chen, Y., Fogel, S., Doyon, J., Wu, J., Xu, J., Zhang, J., Qin, P., Wu, X., Mao, Y., Mashour, G. A., Hudetz, A. G., & Northoff, G. (2020). Altered global brain signal during physiologic, pharmacologic, and pathologic states of unconsciousness in humans and rats. *Anesthesiology*, *132*(6), 1392–1406.

Tononi, G. (2004). An information integration theory of consciousness. *BMC Neuroscience*, *5*, 42.

Tononi, G., Boly, M., Massimini, M., & Koch, C. (2016). Integrated information theory: From consciousness to its physical substrate. *Nature Reviews. Neuroscience*, *17*(7), 450–461.

Wang, J. H., Wang, X. D., Xia, M. R., Liao, X. H., Evans, A., & He, Y. (2015). GRETNA: A graph theoretical network analysis toolbox for imaging connectomics. *Frontiers in Human Neuroscience*, *9*, 386.

Xia, M. R., Wang, J. H., & He, Y. (2013). BrainNet viewer: A network visualization tool for human brain Connectomics. *PLoS One*, *8*(7), e68910.

Xu, Z., Liu, F., Yue, Y., Ye, T., Zhang, B., Zuo, M., Xu, M., Hao, R., Xu, Y., Yang, N., & Che, X. (2009). C50 for propofol-remifentanil target-controlled infusion and bispectral index at loss of consciousness and response to painful stimulus in Chinese patients: A multicenter clinical trial. *Anesthesia and Analgesia*, *108*(2), 478–483.

Yan, C., & He, Y. (2011). Driving and driven architectures of directed small-world human brain functional networks. *PLoS One*, *6*(8), e23460.

Yan, C. G., Cheung, B., Kelly, C., Colcombe, S., Craddock, R. C., Di Martino, A., Li, Q. Y., Zuo, X. N., Castellanos, F. X., & Milham, M. P. (2013). A comprehensive assessment of regional variation in the impact of head micromovements on functional connectomics. *NeuroImage*, *76*(1), 183–201.

Yang, Z., Craddock, R. C., Margulies, D. S., Yan, C. G., & Milham, M. P. (2014). Common intrinsic connectivity states among posteromedial cortex subdivisions: Insights from analysis of temporal dynamics. *NeuroImage*, *93*, 124–137.

Yu, Q. B., Erhardt, E. B., Sui, J., Du, Y. H., He, H., Hjelm, D., Cetin, M. S., Rachakonda, S., Miller, R. L., Pearlson, G., & Calhoun, V. D. (2015). Assessing dynamic brain graphs of time-varying connectivity in fMRI data: Application to healthy controls and patients with schizophrenia. *NeuroImage*, *107*, 345–355.

SUPPORTING INFORMATION

Additional supporting information can be found online in the Supporting Information section at the end of this article.

How to cite this article: Li, S., Chen, Y., Ren, P., Li, Z., Zhang, J., & Liang, X. (2023). Highly connected and highly variable: A Core brain network during resting state supports Propofol-induced unconsciousness. *Human Brain Mapping*, *44*(2), 841–853. https://doi.org/10.1002/hbm.26103